

Fiber-optic plasmonic probe with nanogap-rich Au nanoislands for on-site surface-enhanced Raman spectroscopy using repeated solid-state dewetting

Jihyun Kwak
Wonkyoung Lee
Jae-Beom Kim
Sang-In Bae
Ki-Hun Jeong

Fiber-optic plasmonic probe with nanogap-rich Au nanoislands for on-site surface-enhanced Raman spectroscopy using repeated solid-state dewetting

Jihyun Kwak,^{a,b} Wonkyoung Lee,^{a,b,c} Jae-Beom Kim,^{a,b} Sang-In Bae,^{a,b} and Ki-Hun Jeong^{a,b,*}

^aKorea Advanced Institute of Science and Technology (KAIST), Department of Bio and Brain Engineering, Daejeon, Republic of Korea

^bKorea Advanced Institute of Science and Technology (KAIST), KAIST Institute for Health Science and Technology, Daejeon, Republic of Korea

^cElectronics and Telecommunications Research Institute, Daejeon, Republic of Korea

Abstract. We report a fiber-optic plasmonic probe with nanogap-rich gold nanoislands for on-site surface-enhanced Raman spectroscopy (SERS). The plasmonic probe features nanogap-rich Au nanoislands on the top surface of a single multimode fiber. Au nanoislands were monolithically fabricated using repeated solid-state dewetting of thermally evaporated Au thin film. The plasmonic probe shows 7.8×10^6 in SERS enhancement factor and 100 nM in limit-of-detection for crystal violet under both the excitation of laser light and the collection of SERS signals through the optical fiber. The fiber-through measurement also demonstrates the label-free SERS detection of folic acid at micromolar level. The plasmonic probe can provide a tool for on-site and *in vivo* SERS applications. © The Authors. Published by SPIE under a Creative Commons Attribution 4.0 Unported License. Distribution or reproduction of this work in whole or in part requires full attribution of the original publication, including its DOI. [DOI: [10.1117/1.JBO.24.3.037001](https://doi.org/10.1117/1.JBO.24.3.037001)]

Keywords: solid-state dewetting; surface-enhanced Raman spectroscopy; plasmonics; nanofabrication; fiber optics.

Paper 180552R received Sep. 17, 2018; accepted for publication Jan. 2, 2019; published online Mar. 14, 2019.

1 Introduction

In vivo molecular biosensing of disease-related biomarkers enables early diagnosis of diseases, ¹ intraoperative guidance for cancerous tissue removal, ² and monitoring biomarkers of chronic diseases, such as diabetes ³ and atherosclerosis. ⁴ Intrinsically, rare biomolecular detection for such diseases in the complex biological environment is still challenging in *in vivo* molecular diagnostics. ⁵ Surface-enhanced Raman spectroscopy (SERS) allows highly specific and ultrasensitive molecular diagnostics. The substantial enhancement of both an excitation light and Raman scattering of small molecules near electromagnetic hotspots of plasmonic nanostructures results in extraordinary sensitivity of SERS. ⁶ For decades, plasmonic nanostructures on miscellaneous substrates ⁷⁻⁹ have enabled biomedical SERS applications from *in situ* point-of-care testing ¹⁰ to *in vivo* molecular sensing. ³ In particular, labeled plasmonic nanoparticles have been extensively utilized as SERS reporters for the *in vivo* detection and intraoperative guidance of cancerous lesions. ¹¹⁻¹³ However, technical challenges of plasmonic nanoparticles probes, such as labeling of Raman-active molecules, high administered dosage, or toxicity, still remain substantial obstacles for SERS-based *in vivo* molecular detection. ¹⁴

Fiber-optic probes can serve as minimal invasive, flexible, and biocompatible sensing platforms for detecting optical signals from biochemical molecules in a remote location. ¹⁵ Implementation of plasmonic nanostructures on a fiber-top surface provides an ideal nanoplatform for *in vivo* SERS biosensing. ¹⁶ Recently, plasmonic fiber-optic probes for SERS were fabricated on the top surface with precisely defined metallic nanostructures using nanolithographic methods. ^{17,18} Furthermore, the direct implementation of the nanostructures

has been achieved on the fiber-top surface using oblique angle deposition ¹⁹ or subsequent thermal annealing. ²⁰ However, a cost-effective nanofabrication of biocompatible Au nanostructures on fiber-top surfaces with quantitative analysis is still under development for utilizing plasmonic fiber-optic probe as an *in vivo* SERS sensor.

Here, we report a plasmonic fiber-optic probe with nanogap-rich Au nanoislands on the fiber-top surface using repeated solid-state dewetting. Figure 1(a) illustrates the schematic diagram of the fiber-optic plasmonic probe. An excitation laser of 633 nm is coupled through the end of a multimode fiber (MMF), and surface-enhanced Raman scattering of small biomolecules near the SERS-active fiber-top surface is collected through the same fiber. Figure 1(b) shows the schematic illustration of Au nanoislands on the plasmonic fiber optic. Repeated solid-state dewetting effectively constructs nanogap-rich Au nanoislands on the fiber-top surface, which induce strong electromagnetic (EM) hotspots and thus enable strong light excitation as well as highly sensitive SERS detection of biomolecules through the plasmonic probe.

2 Design and Batch Nanofabrication

Standard multimode silica optical fibers [Thorlabs, FG105LCA, numerical aperture (NA) 0.22] were used for the nanofabrication procedures. SERS signals on the fiber-top surface radiatively scatter in all directions and thus an MMF is highly suitable for high photon collection, compared to a single-mode fiber (SMF) with low NA. ¹⁷ The percentage of total scattered light collected on the top surface of both SMF and MMF was calculated for the maximum collection efficiency of SERS signals. ¹⁷ The percentage of collected total SERS signals of MMF (~1.2%) is about 4.9 times higher than the that of SMF (Thorlabs, SM600, NA 0.1) (~0.25%) under the same condition. In addition, MMF of low-OH (hydroxyl) content pure silica core with acrylate coating was used for the minimum Raman

*Address all correspondence to Ki-Hun Jeong, E-mail: kjeong@kaist.ac.kr

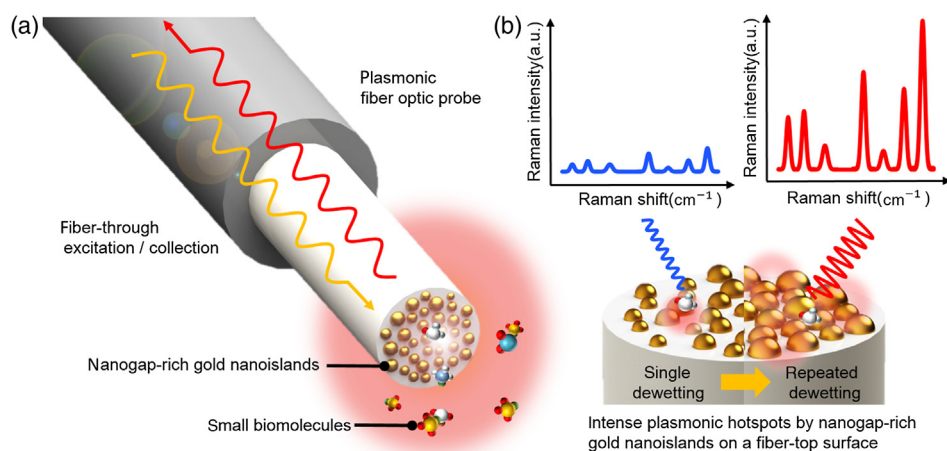


Fig. 1 Fiber-optic plasmonic probe for SERS with nanogap-rich Au nanoislands on the top surface of a MMF. (a) A schematic illustration of the plasmonic probe, where both the laser excitation and the collection of SERS signals are transmitted through a multimode optical fiber. (b) Plasmonic Au nanoislands on the fiber-top surface fabricated using a single or repeated solid-state dewetting of thin Au film. The repeated solid-state dewetting simply creates nanogap-rich Au nanoislands with highly dense and strongly coupled EM fields, i.e., plasmonic hotspots, and thus allow strong light excitation as well as highly sensitive SERS detection of biomolecules, compared to the single dewetting.

background noise.²¹ In the experiment, acrylate coating of each fiber was first removed using a fiber stripper and isopropyl alcohol to avoid thermal degradation. A compact automated fiber cleaver (Vytran[®], LDC401A) was used for preparing 15-cm-long optical fibers with a smooth fiber-top surface. The optical

fibers were fixed on a home-built batch-loading mount ($60 \times 30 \times 2 \text{ mm}^3$) designed for aligning the top surfaces of fibers normal to an Au target source in a thermal boat of an evaporator, as shown in Fig. 2(a). Thin Au film was directly evaporated on the fiber-top surfaces at 1 \AA/s in deposition

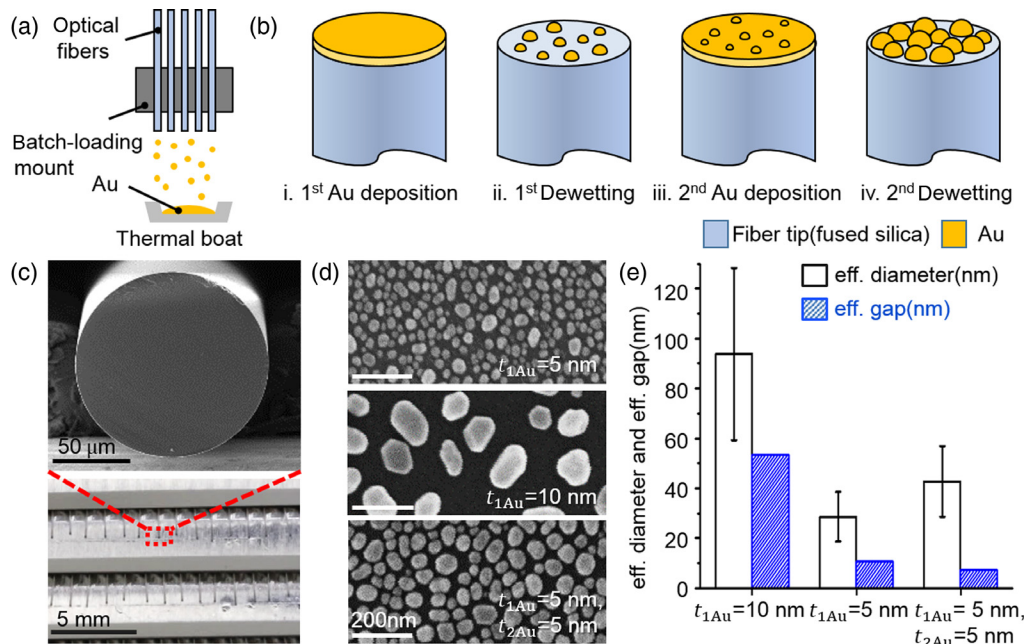


Fig. 2 Nanofabrication procedure for fiber-optic plasmonic SERS probe. (a) A batch-loading mount for multiple optical fibers, which can be placed on the loading chuck of thermal evaporator. (b) Nanofabrication procedures of nanogap-rich Au nanoislands on a fiber-top surface using repeated solid-state dewetting of thin Au film. (c) A SEM image of the fabricated plasmonic fiber-optic probe (top) and an optical image of multiple plasmonic probes on the batch-loading mount (bottom). (d) SEM images of Au nanoislands on the fiber-top surfaces using single or repeated dewetting of different initial thin Au film thickness. Au nanoislands by single dewetting for 5- and 10-nm film thicknesses denoted by $t_{1Au} = 5$ and 10 nm , respectively, and those of repeated dewetting for initial and additional 5-nm thicknesses of Au films denoted by $t_{1Au} = 5 \text{ nm}$ and $t_{2Au} = 5 \text{ nm}$. (e) Effective diameters and effective gap size of Au nanoislands for each fabrication condition extracted from the SEM.

rate under the chamber pressure of 5×10^{-5} torr. Subsequently, the fibers were detached from the mount and arranged on a quartz wafer without any adhesive for thermal annealing in a box furnace. Solid-state dewetting of thin Au film on the fiber-top surfaces was done by thermal annealing in the box furnace at 500°C for 1 h, as shown in Fig. 2(b). Figure 2(c) shows a scanning electron microscopic (SEM) image of the fabricated fiber-optic plasmonic probe (top) and an optical image of the multiple plasmonic probes on the batch-loading mount (bottom). The experiment results in Fig. 2(d) confirm that the effective gap of Au nanoislands becomes clearly narrow after the repeated dewetting compared to the single dewetting for a constant total film thickness.⁸ Figure 2(e) shows the effective diameter and gap size of Au nanoislands depending on the initial Au thickness. The physical dimension of the effective diameter and gap was precisely extracted from the binary formats of each SEM images [region of interest (ROI): $550 \times 550 \text{ nm}^2$] for Au nanoislands on the fiber top using ImageJ[®] software. Assuming the same number of “unit cells” as the number of Au nanoislands in ROI, each Au nanoislands with “effective diameter” is included in each unit cell and the “effective gap” is defined by subtracting the effective diameter from the width of a unit cell. For a constant Au thickness of 10 nm, the Au nanoislands after single dewetting clearly show a much

larger standard deviation for the effective diameter than that of repeated dewetting [Fig. 2(e)]. In addition, it is also confirmed that the effective gap between Au nanoislands fabricated by the repeated dewetting is narrower than that of single dewetting of $t_{1\text{Au}} = 5 \text{ nm}$. As a result, Au nanoislands from the repeated dewetting create strong and uniform plasmonic hotspots due to the large diameter and narrow gap²² with low standard deviation, compared to those from the single dewetting.

3 Plasmonic Properties of Au Nanoislands on the Fiber-Top Surfaces

Both incident light and Raman scattering of molecules are strongly enhanced in the localized EM fields, i.e., hotspots, near Au nanoislands and significantly contribute to EM enhancement of SERS signals.²³ Figures 3(a) and 3(b) show the electric field distribution of fabricated Au nanoislands depending on the initial thin Au film thickness was numerically calculated at an excitation wavelength of 633 nm using the finite-difference time-domain (FDTD) method for the extruded three-dimensional models of the binary image. The individual Au nanoislands were considered as a cylindrical shape and the height was set to the total thickness of Au film. The enhanced E -field clearly shows a large area for the Au nanoislands from repeated dewetting of $t_{1\text{Au}} = 5 \text{ nm}$ and $t_{2\text{Au}} = 5 \text{ nm}$

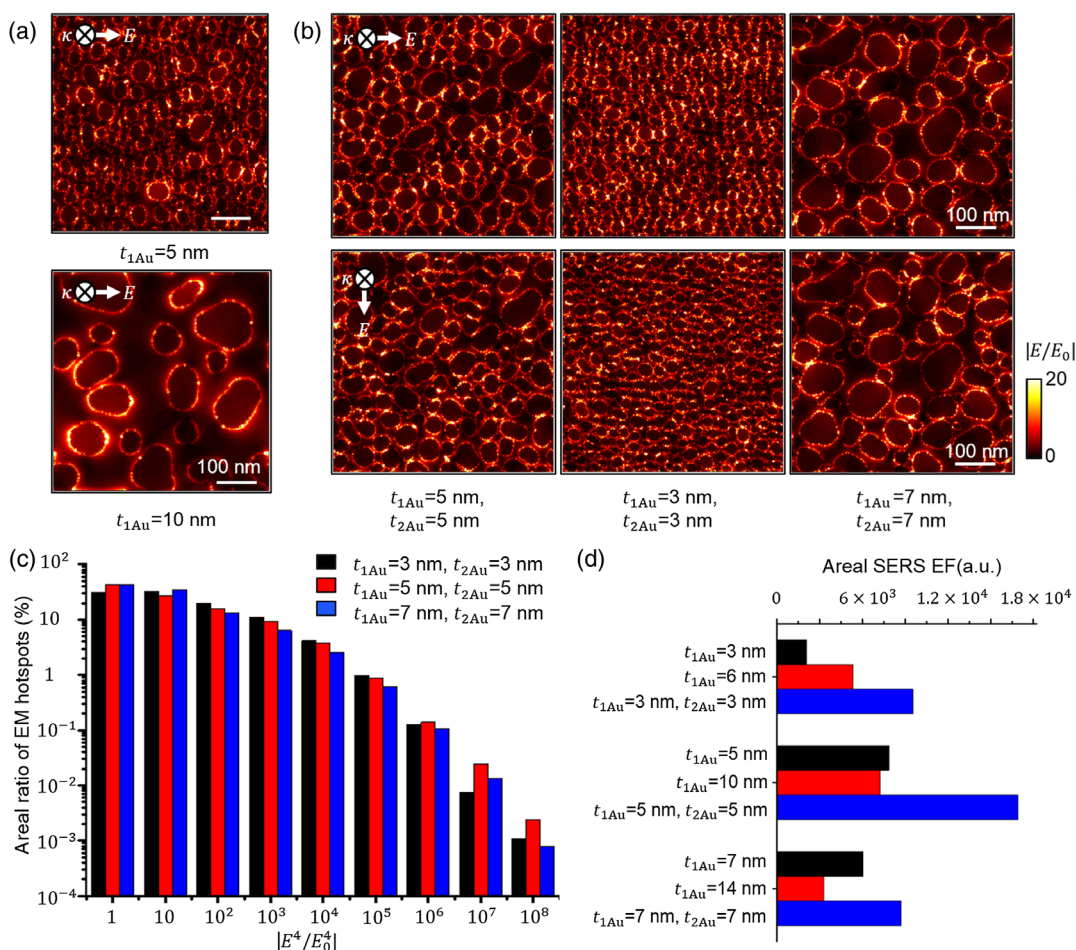


Fig. 3 Plasmonic properties of nanogap-rich Au nanoislands on fiber-top surfaces. (a) The calculated electric field distribution of Au nanoislands obtained from (a) single dewetting and (b) repeated dewetting using the FDTD method. (c) Areal ratio of hotspots for the total enhanced E -field enhancement. (d) Areal SERS EFs of Au nanoislands depending on the initial thicknesses of Au thin film.

[Fig. 3(b)], compared to those from the single dewetting of $t_{1\text{Au}} = 10 \text{ nm}$ [Fig. 3(a)]. Figure 3(b) also clearly demonstrates the E -field between the Au nanoislands is localized along the direction of E -field polarization. In addition, the “hottest” sites of extraordinary strong EM fields compared to other hotspots largely contribute to total SERS signals.^{8,23,24} In this perspective, the areal ratio of EM hotspots to the total enhanced E -field substantially contributes to the enhancement of SERS signals. Figure 3(c) shows that Au nanoislands from the repeated dewetting clearly show a large areal ratio of “hottest sites,” i.e., hotspots with EM enhancement over 10^7 , compared to those from single dewetting. The areal SERS enhancement factor (EF) was introduced to compare the average EM enhancement for Au nanoislands over the ROI ($550 \times 550 \text{ nm}^2$) because the hottest sites exist in a small fraction of the total ROI. The areal SERS EF was calculated by integrating the fourth power of enhanced E -fields over an incident E -fields within the ROI.²⁵ Figure 3(d) clearly shows that the repeated dewetting for $t_{1\text{Au}} = 5 \text{ nm}$ and $t_{2\text{Au}} = 5 \text{ nm}$ has the maximum areal SERS EF, comparable to the single dewetting conditions as well as other repeated dewetting conditions.

4 Fiber-Through SERS Measurement

The SERS EFs for plasmonic probes were first measured on the fiber-top surface depending on the repeated dewetting condition as shown in Fig. 4(a). In the experiment, the fiber tips were immersed for 12 h in a 3 mM BT (Sigma-Aldrich) in methanol.

The SERS signals of BT were measured using He-Ne laser (Thorlabs, $\lambda = 632.8 \text{ nm}$, 0.46 mW) and a spectrometer (Princeton Instruments, MicroSpec 2300i) with an inverted microscope (Zeiss, Axiovert 200 M, objective lens NA = 0.5). Direct excitation onto BT molecules adsorbed on the fiber-top surface of plasmonic probe and collection of the SERS signals were done with the objective lens. The intensity of the 1069-cm^{-1} peak of BT molecules from the SERS and Raman measurements was used to calculate the SERS EF, i.e., $\text{EF} = (I_{\text{SERS}}/N_{\text{SERS}})/(I_{\text{Raman}}/N_{\text{Raman}})$.²⁶ As a result, the SERS EF for the plasmonic probe resulting from repeated dewetting for $t_{1\text{Au}} = 5 \text{ nm}$ and $t_{2\text{Au}} = 5 \text{ nm}$ was 7.8×10^6 , which is increased by 10.4 times compared to that from the single dewetting. The experimental results match with numerically calculated areal SERS EFs in Fig. 3(d). In particular, repeated dewetting for $t_{1\text{Au}} = 5 \text{ nm}$ and $t_{2\text{Au}} = 5 \text{ nm}$ has less densely distributed Au nanoislands compared to those for $t_{1\text{Au}} = 3 \text{ nm}$ and $t_{2\text{Au}} = 3 \text{ nm}$ [Fig. 3(a)]. However, the enlarged Au nanoislands have high polarizability and high coupled dipole EM fields of nanoislands and thus result in high plasmonic enhancement for SERS signals.²² Finally, the plasmonic probe from the repeated dewetting of $t_{1\text{Au}} = 5 \text{ nm}$ and $t_{2\text{Au}} = 5 \text{ nm}$ was utilized for the fiber-through SERS measurements of crystal violet (CV) and folic acid (FA). Figure 4(b) shows an experimental setup for the fiber-through SERS measurement. An excitation laser beam ($\lambda = 632.8 \text{ nm}$, 5.4 mW) was delivered to the fiber-top surface by coupling on the bare surface of plasmonic probe with an objective lens (Zeiss,

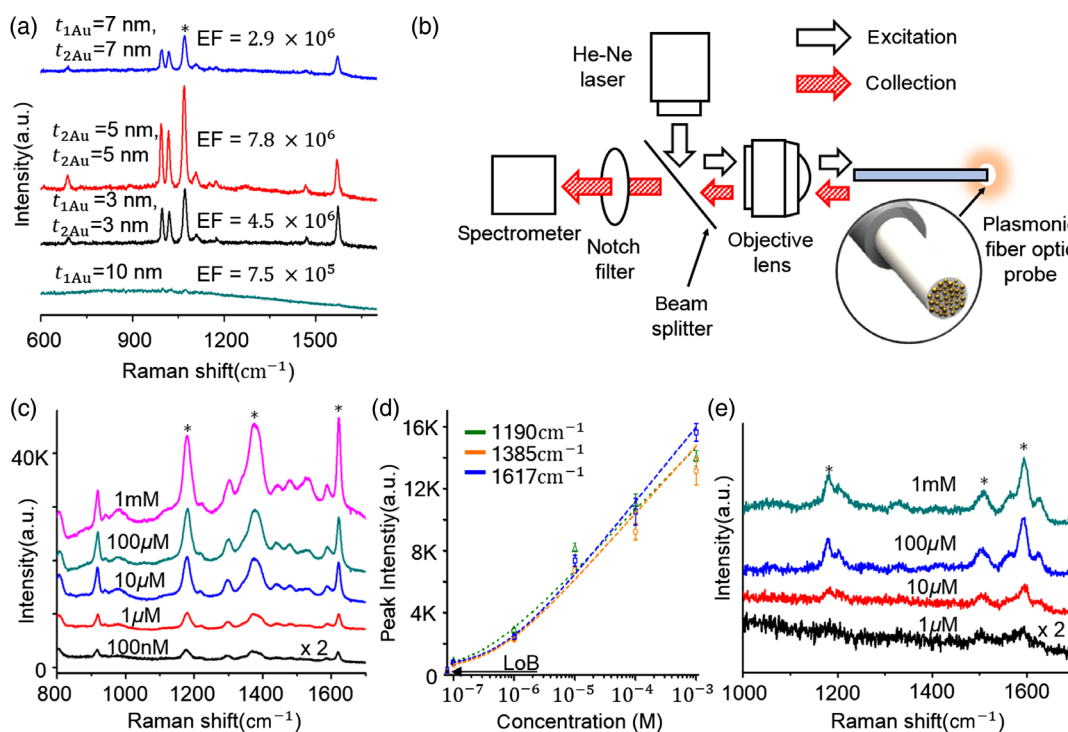


Fig. 4 SERS EFs and fiber-through SERS measurements. (a) SERS EFs for Au nanoislands on the fiber-top surfaces depending on the repeated dewetting conditions. (b) A schematic diagram of experimental setup for fiber-through SERS measurement. Both laser excitation and collection of SERS signals are coupled through the fiber-optic plasmonic probe. (c) Measured SERS signals through the plasmonic fiber ($t_{1\text{Au}} = 5 \text{ nm}$ and $t_{2\text{Au}} = 5 \text{ nm}$) depending on different concentrations of CV molecules. (d) Quantitative SERS measurements of CV molecules using the plasmonic fiber-optic probe. Each SERS peak of CV molecules increases with the concentration of CV molecules. (e) Measured SERS signals of 1 μM FA, well-known as a cancer biomarker.

NA = 0.3). The acquisition time was 10 s for SERS spectra during all the measurement. Raw spectrum of SERS signal from fiber-through SERS measurement exhibits Raman background noise due to the optical fiber because an excitation laser is guided through the optical fiber, similar to previous works.^{17,27} The calibration was then done for all spectra obtained by the fiber-through SERS measurement as follows: a reference spectrum without analytes (deionized water for CV, sodium hydroxide solution 0.1N for FA) and raw SERS spectrum with analytes were initially obtained, and then normalized SERS spectrum with the minimum Raman background signals was taken by subtracting the reference spectrum from the raw SERS spectrum. The normalized SERS spectrum was used in all experiments, as shown in Figs. 4(c)–4(e). Meanwhile, speckle noise signals from an excitation laser were observed during the fiber-through measurement of an MMF for the laser excitation and the SERS measurement. However, the effect of speckle noise on SERS signal was not significantly considered due to both signal reduction of excitation and collection through a short-length MMF (15 cm in length) are negligible.²⁷ Figure 4(c) shows SERS spectra of CV molecules with different concentration in the range of 100 nM to 1 mM. CV often serves as a reference molecule to evaluate the performance of diverse SERS substrates.²⁸ The plasmonic probes were prepared by immersing fiber-top surface in CV (Sigma-Aldrich) in distilled water for 1 min without additional drying process. Representative SERS peaks of CV and their relative standard deviation (RSD) are shown in Figs. 4(c)–4(d). These SERS peaks of CV at 915, 1190, 1385, and 1617 cm^{-1} are originated from ring skeletal vibrations, such as C–H in plane bending, N-phenyl stretching, and C–C stretching.²⁹ The limit-of-detection (LOD) was calculated by the summation of limit-of-blank (LoB) and critical standard deviation of the target molecule.³⁰ The LoB obtained from the SERS signal of deionized water (blank solution) and 100 nM CV samples in three representative SERS peaks are shown in Fig. 4(d). The plasmonic fiber-optic probe exceptionally shows the LOD of 100 nM for the SERS measurement of CV, compared to previously reported works.^{28,31} In addition, the reproducibility of SERS signals was also evaluated by performing the SERS measurement of 1 μM CV measurement using eight plasmonic probes from different batches under the same fabrication conditions. The RSD was calculated from the SERS signals from four representative Raman peaks of CV.²⁹ The RSD in SERS signals of the proposed plasmonic probe shows 8.87% in average whereas the SERS probe fabricated by anodic alumina oxide is 9.60% in RSD.³² Figure 4(e) shows the SERS spectra for FA based on the fiber-through measurement. FA molecules play an important role for cell synthesis in facilitating one-carbon metabolism of amino acid in the body. In particular, FA serves as a well-known biomarker of cancers because folate receptors are overexpressed in the membranes of most cancer cell lines, such as epithelial, breast, ovary, lung, and brain.³³ As a result, *in vivo* deficiency and low concentration of FA can be utilized for cancer diagnosis³⁴ and drug delivery monitoring with FA-conjugated nanocarriers.³⁵ In the experiment, the plasmonic probes were prepared by immersing in FA (Sigma-Aldrich) solution (0.1N NaOH, Sigma-Aldrich) in aforementioned manner. The experimental results clearly demonstrate that the fiber-through SERS measurement allows the label-free detection of FA molecules at micromolar level.

5 Summary

In summary, we have successfully demonstrated the fiber-optic plasmonic probe with nanogap-rich Au nanoislands for highly sensitive SERS of biomolecules. The plasmonic probe was batch fabricated using repeated dewetting of thin Au film. The plasmonic probe shows 7.8×10^6 in SERS EF and 100 nM in LOD for CV through the fiber-through measurement. In addition, the plasmonic fiber has also successfully demonstrated the SERS detection of FA at micromolar level. The plasmonic probe can provide a tool for diverse on-site and *in vivo* SERS applications.

Disclosures

Authors have no relevant financial interests in the paper and no other potential conflicts of interest to disclose.

Acknowledgments

This work was supported by the National Research Foundation of Korea (NRF) Ministry of Science, ICT and Future Planning (Nos. 2018029899 and 2018018122), and the Ministry of Health and Welfare, Republic of Korea (No. HI16C1111).

References

1. V. W. Davis et al., "Metabolomics and surgical oncology: potential role for small molecule biomarkers," *J. Surg. Oncol.* **103**(5), 451–459 (2011).
2. D. Ghosh et al., "Deep, noninvasive imaging and surgical guidance of submillimeter tumors using targeted M13-stabilized single-walled carbon nanotubes," *Proc. Natl. Acad. Sci. U. S. A.* **111**(38), 13948–13953 (2014).
3. D. A. Stuart et al., "Glucose sensing using near-infrared surface-enhanced Raman spectroscopy: gold surfaces, 10-day stability, and improved accuracy," *Anal. Chem.* **77**(13), 4013–4019 (2005).
4. P. Conti and Y. Shaik-Dasthagirisab, "Atherosclerosis: a chronic inflammatory disease mediated by mast cells," *Cent. Eur. J. Immunol.* **40**(3), 380–386 (2015).
5. A. I. Henry et al., "Surface-enhanced Raman spectroscopy biosensing: *in vivo* diagnostics and multimodal imaging," *Anal. Chem.* **88**(13), 6638–6647 (2016).
6. P. L. Stiles et al., "Surface-enhanced Raman spectroscopy," *Ann. Rev. Anal. Chem.* **1**, 601–626 (2008).
7. M. Park, B. H. Kang, and K. H. Jeong, "Paper-based biochip assays and recent developments: a review," *Biochip J.* **12**(1), 1–10 (2018).
8. M. Kang, S. G. Park, and K. H. Jeong, "Repeated solid-state dewetting of thin gold films for nanogap-rich plasmonic nanoislands," *Sci. Rep.* **5**, 14790 (2015).
9. S. Park, J. Lee, and H. Ko, "Transparent and flexible surface-enhanced Raman scattering (SERS) sensors based on gold nanostar arrays embedded in silicon rubber film," *ACS Appl. Mater. Interfaces* **9**(50), 44088–44095 (2017).
10. M. Park et al., "Plasmonic schirmer strip for human tear-based gouty arthritis diagnosis using surface-enhanced Raman scattering," *ACS Nano* **11**(1), 438–443 (2017).
11. S. Y. Feng et al., "Nasopharyngeal cancer detection based on blood plasma surface-enhanced Raman spectroscopy and multivariate analysis," *Biosens. Bioelectron.* **25**(11), 2414–2419 (2010).
12. D. Lin et al., "Colorectal cancer detection by gold nanoparticle based surface-enhanced Raman spectroscopy of blood serum and statistical analysis," *Opt. Express* **19**(14), 13565–13577 (2011).
13. X. M. Qian et al., "In vivo tumor targeting and spectroscopic detection with surface-enhanced Raman nanoparticle tags," *Nat. Biotechnol.* **26**(1), 83–90 (2008).
14. L. A. Lane, X. M. Qian, and S. M. Nie, "SERS nanoparticles in medicine: from label-free detection to spectroscopic tagging," *Chem. Rev.* **115**(19), 10489–10529 (2015).
15. P. Vaiano et al., "Lab on Fiber Technology for biological sensing applications," *Laser Photonics Rev.* **10**(6), 922–961 (2016).

16. K. I. Mullen and K. T. Carron, "Surface-enhanced Raman-spectroscopy with abrasively modified fiber optic probes," *Anal. Chem.* **63**(19), 2196–2199 (1991).
17. E. J. Smythe et al., "Optical antenna arrays on a fiber facet for in situ surface-enhanced Raman scattering detection," *Nano. Lett.* **9**(3), 1132–1138 (2009).
18. G. F. S. Andrade et al., "Surface-enhanced resonance Raman scattering (SERRS) using Au nanohole arrays on optical fiber tips," *Plasmonics* **8**(2), 1113–1121 (2013).
19. Y. Zhu, R. A. Dluhy, and Y. P. Zhao, "Development of silver nanorod array based fiber optic probes for SERS detection," *Sens. Actuators B-Chem.* **157**(1), 42–50 (2011).
20. A. Dhawan et al., "Nano-engineered surface-enhanced Raman scattering (SERS) substrates with patterned structures on the distal end of optical fibers," *Proc. SPIE* **6869**, 68690G (2008).
21. O. Stevens et al., "Developing fibre optic Raman probes for applications in clinical spectroscopy," *Chem. Soc. Rev.* **45**(7), 1919–1934 (2016).
22. B. N. Khlebtsov et al., "Gold nanoisland films as reproducible SERS substrates for highly sensitive detection of fungicides," *ACS Appl. Mater. Interfaces* **7**(12), 6518–6529 (2015).
23. S. L. Kleinman et al., "Creating, characterizing, and controlling chemistry with SERS hot spots," *Phys. Chem. Chem. Phys.* **15**(1), 21–36 (2013).
24. Y. Fang, N. H. Seong, and D. D. Dlott, "Measurement of the distribution of site enhancements in surface-enhanced Raman scattering," *Science* **321**(5887), 388–392 (2008).
25. P. Pavaskar et al., "A microscopic study of strongly plasmonic Au and Ag island thin films," *J. Appl. Phys.* **113**(3), 034302 (2013).
26. E. C. Le Ru et al., "Surface enhanced Raman scattering enhancement factors: a comprehensive study," *J. Phys. Chem. C* **111**(37), 13794–13803 (2007).
27. M. Xia et al., "SERS optical fiber probe with plasmonic end-facet," *J. Raman Spectrosc.* **48**(2), 211–216 (2017).
28. M. Pisco et al., "Nanosphere lithography for optical fiber tip nanoprobes," *Light: Sci. Appl.* **6**, e16229 (2017).
29. S. L. Smitha et al., "Size-dependent optical properties of Au nanorods," *Prog. Natl. Sci.: Mater. Int.* **23**(1), 36–43 (2013).
30. D. A. Armbruster and T. Pry, "Limit of blank, limit of detection and limit of quantitation," *Clin. Biochem. Rev.* **29**(Suppl. 1), S49–S52 (2008).
31. F. L. Yap et al., "Nanoparticle cluster arrays for high-performance SERS through directed self-assembly on flat substrates and on optical fibers," *ACS Nano* **6**(3), 2056–2070 (2012).
32. X. Liu et al., "Highly uniform and reproducible surface enhanced Raman scattering on air-stable metallic glassy nanowire array," *Sci. Rep.* **4**, 5835 (2014).
33. R. J. Stokes et al., "Surface-enhanced Raman scattering spectroscopy as a sensitive and selective technique for the detection of folic acid in water and human serum," *Appl. Spectrosc.* **62**(4), 371–376 (2008).
34. M. Park, C. S. H. Hwang, and K. H. Jeong, "Nanoplasmonic alloy of Au/Ag nanocomposites on paper substrate for biosensing applications," *ACS Appl. Mater. Interfaces* **10**(1), 290–295 (2018).
35. S. Boca-Farcau et al., "Folic acid-conjugated, SERS-labeled silver nanotriangles for multimodal detection and targeted photothermal treatment on human ovarian cancer cells," *Mol. Pharm.* **11**(2), 391–399 (2014).

Biographies of the authors are not available.